Available online at www.sciencedirect.com
SCIENCE DIRECT®
Acta Materialia 53 (2005) 4237–4244
Acta MATERIALIA
www.actamat-journals.com

Hydraulically pumped cone fracture in brittle solids

Herzl Chai [a], Brian R. Lawn [b,*]

[a] Department of Solid Mechanics, Materials and Systems, Tel Aviv University, Tel Aviv, Israel
[b] Materials Science and Engineering Laboratory, National Institute of Standards and Technology, Building 301, Shipping and Receiving, Gaithersburg, MD 20899-8500, USA

Received 27 April 2005; received in revised form 16 May 2005; accepted 16 May 2005
Available online 11 July 2005

Abstract

An analysis of inner cone cracks in brittle solids subject to cyclic indentation in liquid is presented. These inner cone cracks, so named because they form well within the maximum contact circle, are postulated to be driven by a hydraulic pumping mechanism. Unlike their more traditional outer cone crack counterparts, inner cones do not appear in monotonic loading or even cyclic loading in the absence of liquid. According to the hydraulic pumping postulate, an expanding contact engulfs surface fissures or flaws, closing the crack mouths and squeezing entrapped liquid toward the subsurface tips, thereby enhancing downward penetration. Finite element modeling is used to analyze the stress and displacement fields in the vicinity of the growing cracks and to compute stress-intensity factors, using soda-lime glass loaded by a spherical indenter in water as a case study. A stepwise incrementing procedure determines the inner cone crack evolution, i.e., crack depth c as a function of number of indentation cycles n, for this system. The predicted $c(n)$ response reproduces essential features of experimentally observed behavior, relative to companion outer cone cracks: notably, a sluggish start in the initial regions, where Hertzian stresses govern, followed by rapid acceleration as hydraulic pumping activates, ultimately dominating in the steady-state far-field.
Published by Elsevier Ltd on behalf of Acta Materialia Inc.

Keywords: Contact fracture; Curved surfaces; Cyclic loading; Hydraulic pumping; Inner cone cracks

1. Introduction

The incidence of fracture from contact loading between a thick brittle solid and a curved indenter is a long-standing classical problem, beginning with Hertz in the 1880s [1] and intensifying over the past four decades with the advancement of indentation fracture mechanics [2,3]. Most familiar are the shallow circumferential or "outer" cone or ring fractures that form outside an expanding sphere contact in single-cycle loading: in brittle monoliths the location of these outer surface rings typically lies within 15% of the contact circle [4]; in brittle coating layers on compliant substrates the surface rings migrate much further out from the contact, as a result of superimposed flexural stresses [5]. More recently, with extension of experimentation to cyclic loading in liquid environments, a second kind of cone crack has been observed to form well within the maximum contact circle [6]. These so-called "inner" cone cracks are noticeably steeper and can propagate much deeper after extended cycling, sometimes leading to penetration failure in thinner plates [7]. Examples from an earlier study are shown in Fig. 1 for cyclic loading with a tungsten carbide (WC) spherical indenter on glass and porcelain in water [6]. Inner cones form only in cyclic loading in water, so they cannot be explained by an exclusively time-dependent mechanism such as chemically enhanced slow crack growth in the same way as outer cone cracks [6,8,9]. It would appear that some additional, cumulative mechanical driving force associated with the periodic ingress and egress of liquid must operate [7],

* Corresponding author. Tel.: +1 301 975 5775.
E-mail address: brian.lawn@nist.gov (B.R. Lawn).

1359-6454/$30.00 Published by Elsevier Ltd on behalf of Acta Materialia Inc.
doi:10.1016/j.actamat.2005.05.026

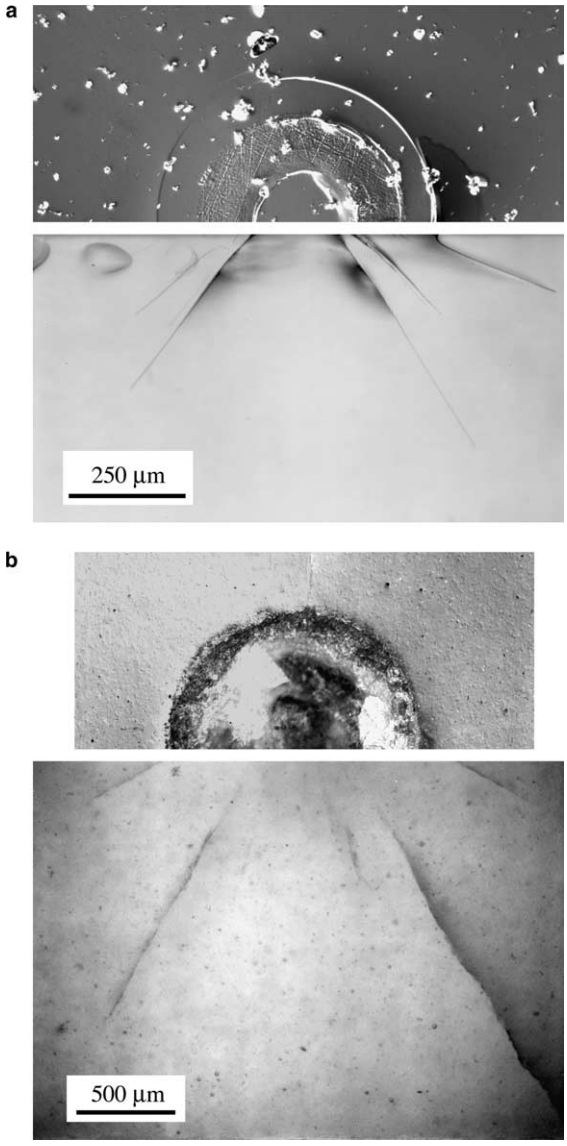

Fig. 1. Cone cracks in brittle material subject to cyclic contact in water with WC spheres of radius $r = 3.18$ mm. Half-surface and section micrographs of cracks in (a) glass (load $P = 140$ N, $n = 10^4$ cycles) and (b) porcelain ($P = 500$ N, $n = 5 \times 10^4$). Shallow outer and steep inner cracks are evident. Fretting zone due to slip at indenter/specimen interface within contact can provide starting flaws for inner cone crack initiation. Micrographs from Kim et al. [6].

somewhat analogous to the pressure-induced infusion of lubricant into pitting cracks in metal surfaces during rolling contact fatigue [10]. Inner cones can become a dominant mode of failure in hard-coating bilayer systems in repetitive contact loading in aqueous solutions, e.g., dental crowns in occlusion function, and are therefore of great interest in biomechanical systems [7].

In this study, we analyze the mechanics of inner cone crack evolution in monolithic brittle solids from cyclic contact loading in liquid. Any such analysis must explain how the inner cones initiate at the specimen surface well within the maximum contact circle and penetrate a highly compressive stress field immediately beneath the expanding contact before reaching the indentation far-field. It must also account for a mechanical driving force on these cracks from intrusive liquid, over and above the usual slow crack growth effects, in order to explain why these cracks are not apparent in cyclic loading in air. The mechanism envisaged is one in which liquid is squeezed into surface fissures toward the subsurface crack tips as the contact engulfs the flaw [11]. This is a complex fracture mechanics problem involving interaction of Hertzian contact and fluid pressure fields, and so we use finite element analysis to obtain numerical solutions for inner cone crack evolution in a specific material under specific cyclic loading conditions – silicate glass cycled with a WC sphere of prescribed radius in water – for which experimental data are available. We will show that a hydraulic pumping model can account for basic data trends. We will also show that once the cone cracks penetrate the near-contact zone and enter a tensile far-field the hydraulic driving force peters out, and the crack growth characteristics asymptotically approach a familiar analytical solution for center-loaded penny cracks driven solely by slow crack growth.

2. Liquid entrapment mechanism

The contact variables of interest are depicted in the schematic of Fig. 2: a spherical indenter of radius r at load P and contact radius a, with maximum values P_m and a_m. The contact is assumed to take place in a liquid environment over n cycles. Cone cracks located a distance R from the contact axis form at an angle α to the top surface and propagate to a length C or depth $c = C\sin\alpha$. Tensile stresses occur outside a drop-shaped compression zone of approximate radius a beneath the indenter, shown as the shaded area in Fig. 2. Outer cone cracks (**O**) form at $R_O \approx 1.15a_m$ with $\alpha_O \approx 22°$ [4], and hence are never subject to compression through the cyclic evolution. Inner cones (**I**) form at $R_I \approx 0.5a_m$ with $\alpha_i \approx 50°$ (Fig. 1), although some variations in these coordinates occur from material to material. This location represents a compromise between counteracting factors: if R_I were to be smaller than $0.5a_m$ then the crack would open at lower loads but there would not be a large volume of entrapped liquid to drive the fracture; if R_I were to be larger than $0.5a_m$ then the volume of entrapped fluid would be larger but the range of contact radius over which this fluid could be forced into the crack before reaching its maximum at a_m would be reduced. The cone angles closely approximate maximum principal stress trajectories in the Hertzian field at maximum contact, implying essentially tensile fracture (mode I) [12]. The inner cones experience small surface tensile stresses prior to engulfment ($a < R_I$, Fig. 3(a)), but much

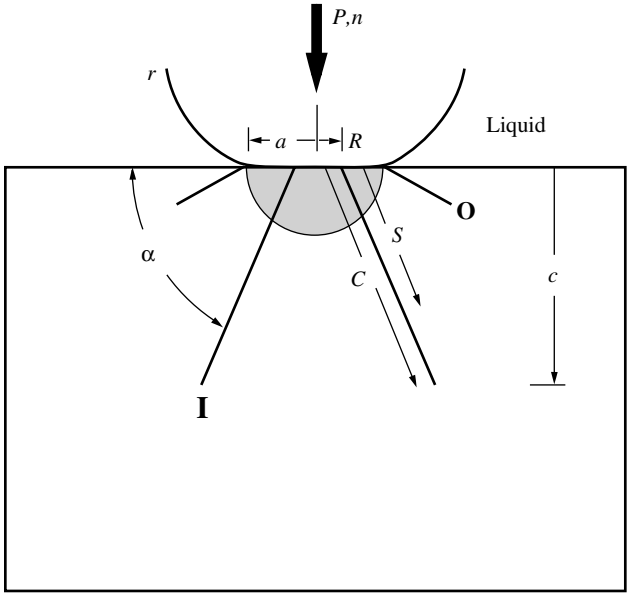

Fig. 2. Schematic of cone crack system in brittle solid. Spherical indenter, sphere radius r, contact radius a, load P and cycles n. Cone cracks of length $c = C\sin\alpha$, angle α to surface, located distance R from contact axis. Label **O** designates outer cones, **I** inner cones. Shaded area indicates compression zone below contact. Contact occurs in liquid. (Linear crack profiles are simplistic representations of actual paths in Fig. 4.)

higher surface compressive stresses after engulfment ($a > R_I$, Fig. 3(b)). However, even inner cones will experience tensile stresses at their extremities after engulfment if they can somehow grow sufficiently large so as to penetrate the compression zone.

We have mentioned that inner cone cracks develop fully only in cyclic loading in liquid, so that there must be some superposed mechanical force associated with liquid intrusion. Consider a starting flaw located at distance R_I from the contact axis on the surface. As the load increases, the contact at first opens the crack, allowing liquid to enter by capillary action (Fig. 3(a)). When the contact circle becomes coincident with the flaw ($a = R_I$), the crack mouth is sealed (although there may exist local fluid reservoirs at the indenter/specimen interface associated with any surface roughness). Further increase in load engulfs the crack ($a \geqslant R_I$), and the crack becomes subject to mouth closure stresses within the drop-shaped compression zone (Fig. 3(b)). Ingress or egress of liquid is then restricted until the indenter is unloaded. Mode I crack opening is induced by fluid pressure by one or both of two possible mechanisms [11]: (i) liquid is forced into surface fissures, providing a wedging force in proportion to the Hertzian pressure; (ii) liquid is forced downward after engulfment in a "pinching" action, closing the crack mouth but opening the tip. The second mode is more consistent with experimental observations where the mouths of well-developed inner cones are observed to close and the far ends open up during loading half-cycles [7].

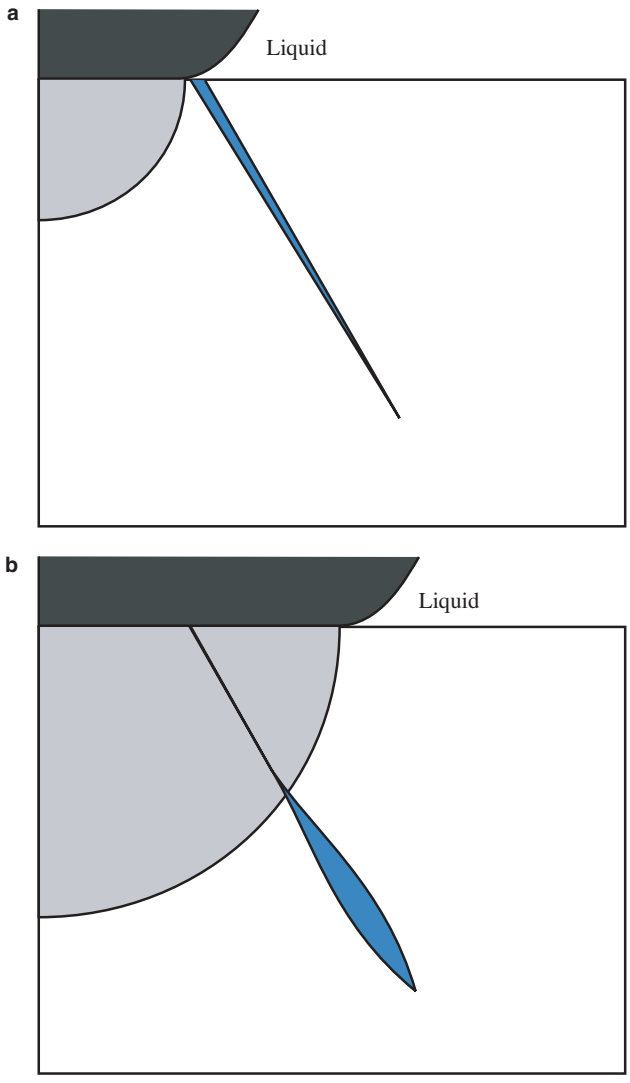

Fig. 3. Schematic demonstrating liquid entrapment model. Shaded area beneath contact designates approximate compression zone. (a) Liquid enter crack prior to contact engulfment. (b) Liquid squeezes toward crack tip as contact expands, causing incremental extension. Cyclic contact repeats process, forcing more liquid into crack in successive cycles.

3. Computation of stress-intensity factors

3.1. FEA model

In the case of outer cone cracks, analytical solutions for incremental cyclic crack growth are available in both the small-flaw initiation and long-crack propagation stages, based on slow crack growth models [6,13]. For inner cones, there currently exist no such analytical solutions, owing to the superposition of complex mechanical driving forces associated with ingressing fluid in the surface cracks.

Accordingly, finite element analysis (FEA) techniques are here used to demonstrate the feasibility of the hydraulic pumping mechanism. The basic FEA

procedure has been outlined in previous studies [5,14]. A flat glass half-space (Young's modulus $E = 70$ GPa and Poisson's ratio $\nu = 0.22$) is indented with a WC sphere ($E = 614$ GPa and $\nu = 0.22$) of radius $r = 1.58$ mm in frictionless axisymmetric contact. In accord with existing experimental data [7], the indenter is loaded in small steps to produce an expanding contact a relative to the surface crack locations R_I and R_O, up to a maximum contact $a_m = 130$ μm at corresponding load $P_m = 120$ N. Calculations are performed for outer and inner cone cracks separately, ignoring any potential interaction between the two. The surface cracks are allowed to extend downward and outward in increments Δc, beginning with short flaws of depth $c = 1$ μm normal to the surface and with $\Delta c \ll c$ at all stages of growth. The mesh is reconfigured at each crack increment, with the grid typically consisting of a minimum 80 equispaced elements along the crack walls (a sufficient number to ensure convergence in the FEA solutions). Stress-intensity factors at each crack depth c are calculated from nodal displacements at the crack walls using the Irwin parabolic crack-tip COD relation [14]. The kink angle α of each crack increment is determined by an angular search algorithm as that which optimizes mode I extension (i.e., $K_{II} = 0$) over the entire load spectrum (i.e., $P \leqslant P_m$). In general, it is found that the cracks follow a somewhat curved path in the small c region, where stress gradients are high, and subsequently straighten out into nearly straight-sided (truncated) cones in the large c region as the cracks approach the far-field. Of course, the angular kink search routine becomes less onerous once the crack straightens out.

These calculations are performed for cracks without and with entrapped fluid, in the latter case by applying superposed uniform normal forces at the nodes along the crack walls to simulate fluid pressure under constant crack volume conditions (fluid incompressibility approximation), as described below.

3.2. Outer cone cracks

First we examine the outer cones. FEA computations for a similar crack system in punch loading have been well described in the literature by Kocer and Collins [15], and we present them here only to confirm the validity of the calculations. Following experimental observation [7], we set $R_O = 1.15a_m = 150$ μm at $P_m = 120$ N. As indicated, the outer cone crack always remains outside the maximum contact circle, with maximum opening at $a = a_m$. In this case, confining fluid pressure is never an issue.

The calculation begins with a normal starting flaw of size $c_O = 1$ μm, commensurate with the scale of small flaws in glass surfaces. The flaw is allowed to increment its depth through a specified amount Δc_O. The algorithm searches for the kink angle α_O that maintains the crack in pure mode I. For outer cones, the maximum K_O is always achieved at maximum load $P = P_m$, where the tensile stress field is greatest. Crack increments are continued sequentially. The crack first forms a shallow collar before curving outward into its characteristic truncated cone geometry. For soda-lime glass, the cone angle in the far-field is $\alpha_O = 22°$. The calculated crack path is indicated by the outer trajectories in Fig. 4.

The function $K_O(c_O)$ for outer cones determined from such calculations is plotted as the uppermost curve in Fig. 5. Note that this curve passes through a maximum at $c_O \approx 8$ μm or $c_O/a_m \approx 0.06$. The broad shape of this curve and position of the maximum are similar to the calculations of Kocer and Collins [15]. Note also that

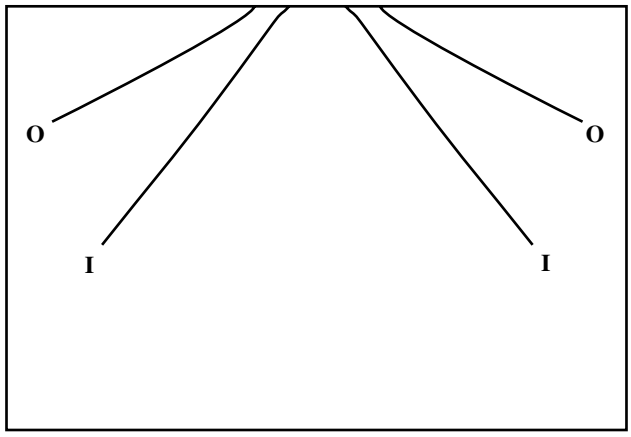

Fig. 4. Calculated crack paths for outer and inner cone cracks in soda-lime glass indented with WC sphere. Note curvature of crack paths near surface, relative steepness of inner cone cracks.

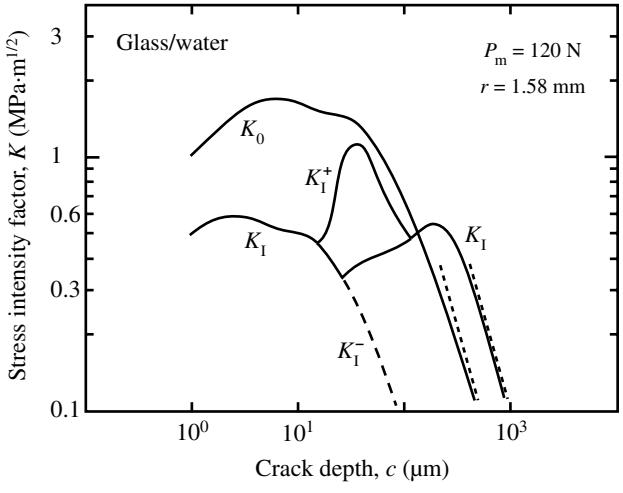

Fig. 5. Mode I stress-intensity factors K as function of crack depth c for glass indented in water with WC sphere. K_O is SIF for outer cone crack. K_I is SIF for inner cone crack without fluid pressure, including contribution from tensile field after engulfment. Dashed curve is equivalent K_I^- with no engulfment. K_I^+ is SIF with fluid pressure included. Dashed lines at right are asymptotic $K \propto c^{-3/2}$ limits for far-field cracks.

the long-crack tail of this curve tends asymptotically to the familiar relation $K_O \propto P/c_O^{3/2}$ (light dashed line) for well-developed cones [2,3].

3.3. Inner cone cracks

3.3.1. Cracks without fluid

For inner cones, we set $R_I = 0.5a_m = 65$ μm for $P_m = 120$ N as per experimental observation [7]. We first perform this calculation in absence of any fluid pressure at the crack walls. Following the procedure in Section 3.2, start with an initial surface flaw at $c_I = 1$ μm and allow stepwise incremental extensions Δc_I. The K terms are computed at each step from the crack-wall nodal displacements behind the tip. The behavior is now more complex, because the configuration of maximum K_I does not necessarily always occur at the engulfment load P_I (Fig. 3(a)), nor at the maximum load P_m (Fig. 3(b)). In other words, inner cone cracks may in some cases continue to extend after first engulfment. To handle this complication, we first retain the angle α_I from the preceding crack increment and determine the load P within $0 \leqslant P \leqslant P_m$ at which $K_{II} = 0$. Then we repeat the computation for various α_I and choose the value of $P = P^*$ that maximizes K_I. For the case study here, this configuration occurs at $P^* < P_m$ for $c_I < 1.5a_m$ and at $P^* = P_m$ for crack depths $c_I > 1.5a_m$ approximately. The calculated crack paths are indicated by the inner trajectories in Fig. 4. As with its outer counterpart, the inner cone crack curves away from normal near the surface, but then straightens out to $\alpha_I \approx 50°$ over the long-crack length for this particular flaw location. The fact that this crack angle is quite different to that of the outer cone beyond the collar region is a manifestation of the fact that the driving force on the crack can indeed continue to increase during the engulfment stage.

The function $K_I(c_I)$ for inner cones without fluid pressure is included in Fig. 5. The dashed curve K_I^- indicates the same function but without engulfment, i.e., stopping the loading at $P = P_I$ (Fig. 3(a)). This latter curve has the same basic shape as K_O but with a downward and leftward shift. The hump in the K_I function at $c_I \approx 20$ μm $= 0.15a_m$ is then due exclusively to additional crack growth beyond engulfment. Again, this is because longer cracks begin to experience some increase in tensile stress intensity in the tip regions as they begin to penetrate the immediate compressive zone. Such additional post-engulfment augmentation, although substantial, is still not large enough to make the inner cone cracks competitive with their outer counterparts in the short-crack region.

3.3.2. Cracks with fluid pressure

Now consider the effect of superposing a fluid pressure on the inner cone crack walls during loading. The sequence of computation is as follows. For any given crack depth c_I and kink angle α_I evaluated in the previous section, determine the crack opening displacements u as a function of coordinate S along the crack path (Fig. 2) immediately prior to first engulfment at $P = P_I$ ($a = R_I$). Calculate the initial crack volume V_0 from the area under the $u(S)$ curve (allowing for the ever-increasing base radius with increasing S). Then increase the load to $P = P^*$ ($a = a^*$), while maintaining fluid volume constant at $V = V_0$ (incompressible liquid). This latter is achieved by introducing equal normal forces over equispaced mesh nodes along the crack walls, equivalent to an internal hydrostatic pressure, starting from zero and incrementing (or decrementing) the forces until the requisite crack volume V_0 is attained. Finally, calculate the stress-intensity factor K_I^+ with superposed fluid pressure from the new nodal displacements.

An example of the change in crack profile for a crack of length $C = 70$ μm (depth $c_I = 50$ μm) and $V = V_0$ is shown in Fig. 6. Note how the crack closes near the mouth in the engulfed crack at $P = P^*$, simultaneously opening up the tip region and thereby enhancing K_I. Note also the parabolic contours close to the crack tip, in accordance with the Irwin crack tip near-field.

The calculations are then repeated for several crack depths c_I, determining a new initial fluid volume V_0 at each c_I. This yields the function $K_I^+(c_I)$ for inner cones with fluid pressure included in Fig. 5. The contribution from hydraulic pressure is thus the differential $\Delta K_I = K_I^+ - K_I$ (not plotted in Fig. 5). An important part of the hydraulic effect is the systematic increase in fluid volume V_0 with each successive cycle, as liquid is continually forced in and out of the crack mouth during unloading and reloading. Hence this contribution is not a factor in monotonic loading (i.e., $\Delta K_I = 0$). Note that

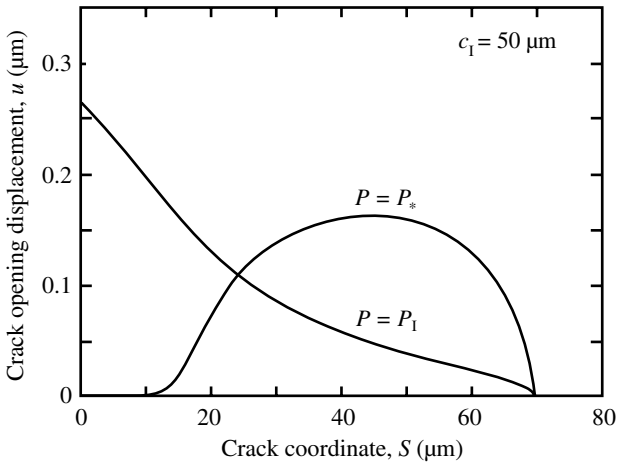

Fig. 6. Crack opening displacements u as function of distance S along crack path for inner cone cracks in glass, without liquid at $P = P_I$ and with liquid pressure at $P = P^*$, volume $V = V_0$, for crack depth $c_I = 50$ μm. Note how mouth closure in second case opens tip region, enhancing field.

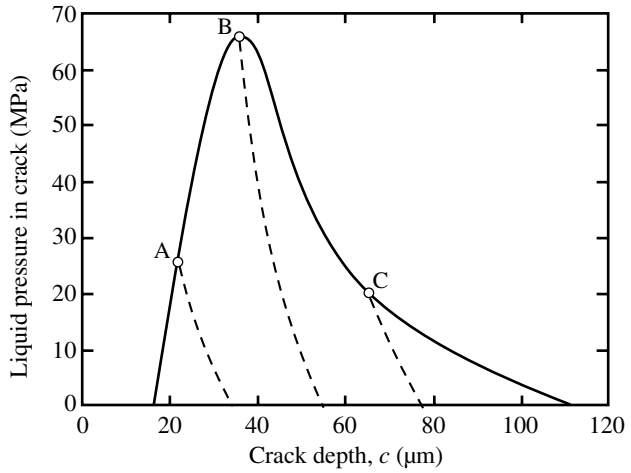

Fig. 7. Fluid pressure in crack. Solid curve is pressure needed to maintain $V = V_0$ at load $P = P^*$ for a crack of fixed depth c. Dashed curves indicate how pressure would diminish if cracks at A, B and C were to be allowed to extend at constant fluid volume and fixed $P = P^*$.

the quantity ΔK_I again does not come into play until $c_I > 17\ \mu m = 0.13 a_m$. (Recall, however, that we are ignoring possible wedging forces from enforced liquid penetration at the Hertzian pressure in this short-crack region.) The hydraulic term ΔK_I considerably enhances the stress-intensity factor in this intermediate crack size region. Such enhancement is evident in Fig. 7 as the plot of the equilibrium fluid pressure needed to maintain $V = V_0$ at load $P = P^*$ as a function of fixed crack depth c, shown as the solid curve. This bell-shaped curve is limited to the region $17\ \mu m < c < 110\ \mu m$, with a maximum at $c = 35\ \mu m$. In principle, once the crack becomes sufficiently large that its tip penetrates beyond $c > 110\ \mu m$ in Fig. 7, corresponding to the region beyond the compression zone at max load P_m (Fig. 3(b)), the fluid pressure can become negative and thereby act to restrain the crack. In reality, the water may be expected to cavitate at this point, effectively wiping out the hydraulic effect. At this stage the inner cone crack is well developed and subject entirely to the Hertzian far-field, with familiar asymptotic $K_I \propto P/c_I^{3/2}$ dependence (dashed line in Fig. 5).

4. Crack extension conditions

Consider now how much crack growth takes place in any given contact cycle. At this stage, it is necessary to introduce a crack extension condition. For growth under equilibrium conditions, extension occurs at $K = K_c$, where K_c is the toughness. However, $K_I^+(c_I)$ in Fig. 5 does not exceed the toughness $K_c = 0.75\ \text{MPa m}^{1/2}$ for soda-lime glass until $c \approx 30\ \mu m$, so small flaws could never extend under such conditions. In reality, crack growth in brittle materials in liquid environments occurs at $K < K_c$ under kinetic conditions, down to K levels below $K_c/3$. This kinetic condition is reasonably well represented by a power law crack velocity relation [16,17]

$$v = v_0 (K/K_c)^N \tag{1}$$

with $N = 17.9$ an exponent and $v_0 = 2.4\ \text{mm s}^{-1}$ a coefficient for soda-lime glass in water [18]. Under these conditions, inner cone cracks represented in Fig. 5 are subject to significant extension.

The velocity equation can then be used to calculate the evolution for outer cone cracks over a number of contact cycles n at frequency f via a seemingly straightforward numerical time-incrementing procedure. The number of cycles Δn to propagate a crack of given depth c_O through $\Delta c_O = v \Delta t \sin\alpha_O$ can be written $\Delta n = f\Delta t/\beta = f\Delta c_O/\beta v \sin\alpha_O$, where the K term used to evaluate v in Eq. (1) is calculated at $P = P^*$ (maximum mode I configuration) and β is a coefficient (<1) to allow for the fact that the crack is not subject to maximum K over an entire cycle [6]. With evaluations of this kind at specific crack lengths, Δn can be integrated numerically to determine $c(n)$.

For inner cone cracks, the procedure becomes more laborious, because the term ΔK_I from fluid pressure is superposed onto the K-field. Recall that this contribution is only important during the intermediate stage of growth in Fig. 5, corresponding to penetration through the compression zone. The complication arises because the entrapped fluid within the inner cone crack walls will be redistributed over a greater crack length as extension proceeds, causing the pressure to relax during extension and thereby diminishing ΔK_I within any single loading cycle. This relaxation is illustrated for three cracks depths (A, B and C) as dashed lines in Fig. 7. To accommodate this relaxation, we adopt the following procedure: (i) as above, for a given initial crack depth c_I, determine the initial crack volume V_0 at first engulfment and calculate K_I at $P = P^*$ while keeping $V = V_0$; (ii) at the selected value of c_I, extend the crack depth in small stepwise increments δc_I at P and V constant, recalculating K_I at each point, as shown in Fig. 8 (how far K_I declines down these curves during any one complete cycle will depend on the loading frequency); (iii) integrate $\delta c_I/v$ in conjunction with Eq. (1) until the condition

$$\int_0^{\Delta c_I} \delta c_I / v \sin\alpha_O = \beta/f$$

is satisfied, thereby identifying the extension Δc_I within a complete cycle; (iv) repeat for selected values of c_I and thereby determine the functional dependence $\Delta c_I(c_I)$; (v) numerically integrate Δc_I over all cycles to determine $c_I(n)$.

The resulting $c_I(n)$ functions for a specific case study, glass/water for maximum load $P_m = 120\ \text{N}$ and frequency $f = 1\ \text{Hz}$, are plotted as the solid lines in

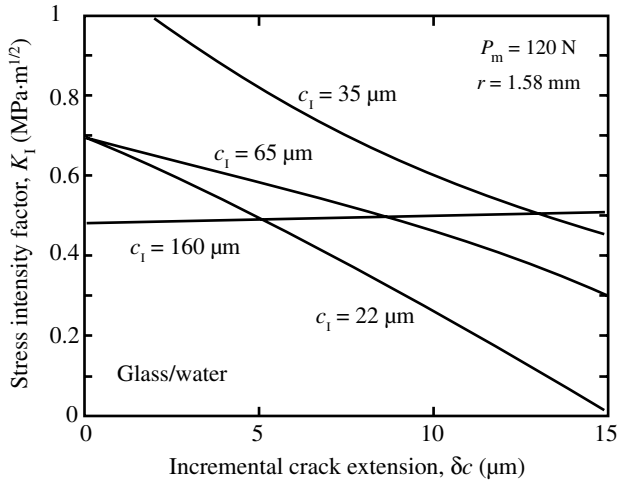

Fig. 8. Plot of $K_I(\delta c_I)$ for selected crack depths c_I for inner cone cracks in glass at fixed load $P = P^*$.

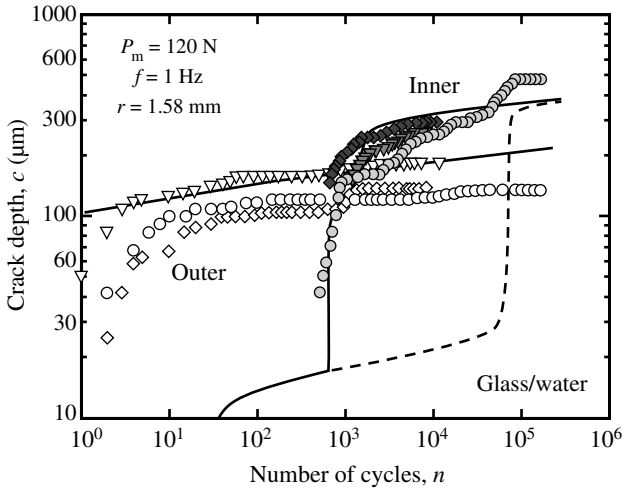

Fig. 9. Predictions of crack evolution functions $c(n)$ for cyclic indentations with WC sphere on soda-lime glass in water, shown as solid curves. Data points are corresponding experimental data (three cracks each mode), filled symbols inner cone cracks and unfilled symbols outer cone cracks [7]. Dashed curve represents growth of inner cone crack in absence of fluid pressure.

Fig. 9. This example is chosen because of availability of corresponding experimental data [7]. Data for outer cone cracks are shown as the unfilled symbols, for inner cone cracks as the filled symbols. The theoretical curves are evaluated using an adjusted $\beta = 0.1$ to give a best fit to these data. The curves reproduce the main trends in the experimental data: for outer cones, initiation within the first cycle, followed by steady growth thereafter into a fully developed cone; for inner cones, relatively slow growth in the initial, short-crack region followed by an abrupt hydraulically driven spurt at $n = 600$ cycles in the intermediate region, slowing finally into a steady growth phase in the long-crack region. This last region tends asymptotically to the far-field limiting dependence $c \propto n^{2/3N}$ ($N = 17.9$), obtained by combining the $K \propto P/c^{3/2}$ relation for center-loaded penny cracks with the velocity function $v \propto K^N$ [6]. The dashed curve in Fig. 9 represents the growth of inner cone cracks without fluid pressure. Note whereas growth is still possible in the absence of hydraulic effects, the predicted growth rate is too slow in relation to observed behavior.

5. Discussion

We have presented a model here, foreshadowed by others [11], of hydraulically assisted crack growth in brittle solids in cyclic contact with spherical indenters in liquids. The cracks of interest are penetrative inner cones within the maximum contact circle, ordinarily not observed in monotonic loading in any environment or in cyclic loading in the absence of liquid. The mechanics are complicated by the fact that the inner cone cracks may continue to grow even after engulfment by the expanding contact, where compressive stresses in the immediate subsurface contact zone act to close the crack mouth yet tensile stresses just beyond this zone open the crack mouth. After an initial period of slow growth from Hertzian stresses alone, liquid entrapment delivers a fluid pressure which drives the crack at an accelerated rate. Continued reloading enables more liquid to enter in successive cycles to build up the pressure with each cycle, counterbalancing the near-contact closure forces. The model envisions progressive squeezing of entrapped liquid towards the subsurface crack tip in a kind of pumping mode, driving inner ring cracks through an otherwise inhibiting compressive contact zone into full cones. Once they penetrate into the far-field the inner cone cracks are driven by remote tensile stresses. Because of the complexity of the cyclic problem, involving periodic crack extension from superposed mechanical and chemical forces, resort to FEA has here been made to evaluate the inner cone evolution. Analysis of a specific case study, that of contact of a glass surface with a WC sphere in water, reproduces the main features of the inner cone evolution in Fig. 9: namely, a slow start relative to its outer cone crack counterpart, but subsequent acceleration with cycling to become the dominant mode of fracture. Ultimately, in the large-crack region all cone cracks, inner and outer, tend asymptotically to a simple far-field limit $c \propto n^{2/3N}$.

The principal value of the present FEA analysis is a demonstration of the feasibility of the hydraulic pumping model. At the same time, we acknowledge certain limitations of the current analysis. We have conducted just one case study, that of a specific material/indenter/environment system. The role of such variables as sphere radius r, maximum load P_m and cyclic frequency f would require a great deal more unwieldy, time-consuming numerical analysis. For this reason, we would

not advocate FEA as means for predicting general behavior. Quite apart from inaccuracies arising from crack increment problems, there are several assumptions that are open to question: (i) The hydraulic model is based entirely on a squeezing mechanism whereby intrusive liquid is forced toward the crack tip by closure stresses at the mouth. We have ignored possible wedging stresses from forced entry of liquid from local reservoirs at a rough indenter/specimen interface into the crack mouth under Hertzian pressure. Such wedging action is more likely to occur in the small flaw region, thereby enhancing and broadening the hump in the K_I^+ curve in Fig. 5. (ii) Possible negative fluid pressures in the long-crack region, where contact engulfment actually acts to increase rather than decrease the confining volume, have been neglected. It has been simply assumed that no such stresses will activate, because of cavitation of the entrapped liquid. In reality, cavitation will not occur until the negative pressure has achieved some non-zero value, thereby acting to inhibit the crack extension in this region. (iii) A fixed location $R_I = 0.5a_m$ has been assumed for the inner surface ring. This midway location balances counteracting factors: higher R_I/a_m would increase the stress intensity acting on the surface flaws prior to engulfment; lower R_I/a_m would increase the stress intensity after engulfment. (iv) Interactions between the inner cone and preceding outer cone have been ignored in the computation. Such interactions could reduce the K-field on an adjacent inner cone crack, further contributing to a shift toward lower R_I/a_m. (v) An attempt has been made to maintain small crack increments, especially in the short-crack region. Stress inhomogeneities are extremely large in this region, so inaccuracies in the increment size and angle are likely to be greatly magnified in the resultant K determinations [19]. Consideration of these factors as a whole suggests that our calculations, if anything, probably underestimate the scale of the hydraulic pumping effect.

The crack law used here to describe the rate dependence of crack growth is the power-law velocity function $v(K)$ in Eq. (1) [17]. Such a function is able to account wholly for the fatigue responses of outer cone cracks [6]. In principle, we may apply the same law to systems in any liquid environment, simply by changing the exponent and coefficient in this function. However, a simple-power law relation does not hold for all liquids, e.g., alkanes, where the $v(K)$ curve exhibits multiple branches, attributable to diffusion rates of trace water within the alkane liquids [20]. This simply means that the time integration over the indentation cycling would have to be conducted entirely numerically. Some materials like silicon are not susceptible to slow crack growth at all. The inner cone cracks could extend only if the $K_I^+(c)$ curve in Fig. 5 were to exceed K_c. In principle, any fatigue would then be solely mechanical, from the hydraulic pumping effect alone, i.e., from continual cyclic augmentation of the entrapped fluid volume V_0 within the crack walls. Such equilibrium growth could in principle be induced by increasing the applied load to extremely high values, manifested in Fig. 5 as a scaling up of the $K_I^+(c)$ curve.

The inner cones, by virtue of their steep angles to the surface, can become a dominant mechanism of failure in thin specimens or in bilayers, e.g., dental crowns [7]. Extension of the current analysis to that case is under way.

Acknowledgments

We acknowledge useful discussions with Sheldon Wiederhorn, Yu Zhang, Yeon-Gil Jung and Sanjit Bhowmick. This work was supported by a grant from the U.S. National Institute of Dental and Craniofacial Research (PO1 DE10976).

References

[1] Hertz H. Hertz's miscellaneous papers. London: Macmillan; 1896 [chapter 5–6].
[2] Lawn BR, Wilshaw TR. J Mater Sci 1975;10:1049.
[3] Lawn BR. J Am Ceram Soc 1998;81:1977.
[4] Wilshaw TR. J Phys D: Appl Phys 1971;4:1567.
[5] Chai H, Lawn BR, Wuttiphan S. J Mater Res 1999;14:3805.
[6] Kim DK, Jung Y-G, Peterson IM, Lawn BR. Acta Mater 1999;47:4711.
[7] Zhang Y, Kwang J-K, Lawn BR. J Biomed Mater Res: B 2005;73B:186.
[8] Padture NP, Lawn BR. J Am Ceram Soc 1995;78:1431.
[9] Zhang Y, Bhowmick S, Lawn BR. J Mater Res (in press).
[10] Way S. J Appl Mech 1935;2:49.
[11] Bower AF. J Tribol 1988;110:704.
[12] Frank FC, Lawn BR. Proc Roy Soc Lond 1967;A299:291.
[13] Lee C-S, Kim DK, Sanchez J, Miranda P, Pajares A, Lawn BR. J Am Ceram Soc 2002;85:2019.
[14] Chai H. Acta Mater 2005;53:487.
[15] Kocer C, Collins RE. J Am Ceram Soc 1998;81:1736.
[16] Wiederhorn SM. J Am Ceram Soc 1967;50:407.
[17] Wiederhorn SM, Bolz LH. J Am Ceram Soc 1970;53:543.
[18] Marshall DB, Lawn BR. J Am Ceram Soc 1980;63:532.
[19] Lawn BR, Wilshaw TR, Hartley NEW. Int J Fract 1974;10:1.
[20] Freiman SW. J Am Ceram Soc 1975;58:339.